Prediction of the tensile strength of FDM specimens based on Tsai Hill criteria

Cosmin Florin Popa, Sergiu Valentin Galatanu
University Politehnica Timisoara, Romania
cosmin.popa@upt.ro, https://orcid.org/0000-0001-8046-4523
sergiu.galatanu@upt.ro, https://orcid.org/0000-0002-7629-8662

Liviu Marsavina
University Politehnica Timisoara, Romania; Romanian Academy – Timisoara Branch, Romania
liviu.marsavina@upt.ro, https://orcid.org/0000-0002-5924-0821

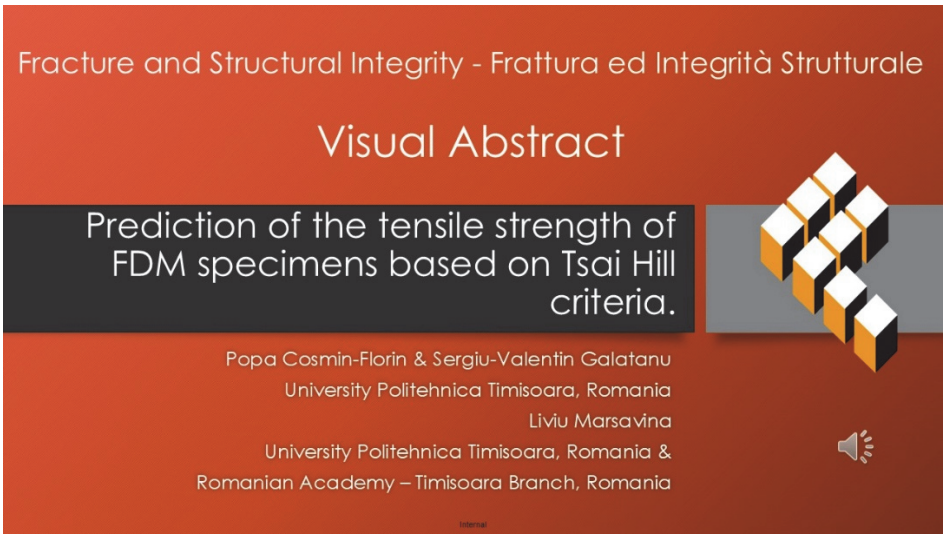

Citation: Popa, C. F., Galatanu, S. V., Marsavina, L., Prediction of the tensile strength of FDM specimens based on Tsai Hill criteria, Fracture and Structural Integrity, 73 (2025) 153-165.

Received: 08.03.2025
Accepted: 20.05.2025
Published: 22.05.2025
Issue: 07.2025

KEYWORDS. FDM, Tsai Hill criteria, PETG, DIC, Mechanical behaviour.

INTRODUCTION

Additive Manufacturing (AM) is a technique that creates complex components by building them layer by layer in a quick and efficient way, without requiring extra post-processing steps to finalize the part [1]. This approach has found broad use in various sectors, such as biomedical engineering [2, 3] and mechanical engineering [4 - 6]. Additive Manufacturing (AM) includes various 3D printing techniques, with this paper specifically focusing on Fused Deposition Modeling (FDM) due to its simplicity, speed, and low material waste. The process of creating a component using FDM consists of several stages, beginning with the creation of a digital 3D model. This model is then loaded into 3D printing software, where parameters such as print speed, bed temperature, nozzle temperature, and raster orientation are set. After configuring the parameters, a G-code file is generated and sent to the 3D printer. The printing process involves feeding a filament through two rollers into a heated nozzle, which melts the material at the designated temperature to build the part layer by layer. In the literature, several researchers have studied the impact of raster orientation on the mechanical properties of 3D-printed specimens, [7]. For example, some have observed significant variations in tensile strength based

on raster orientation. Their findings showed improved tensile properties as the raster angle increased from 30° to 90° [8 - 10].
Regarding shear specimens, other researchers [11, 12, 13] have extensively analyzed the homogeneity of the shear zone and identified in-plane simple shear with a single shear zone as an effective technique for determining shear strength and analyzing in-plane plastic anisotropy.
In [14], it is highlighted that any anisotropy in shear specimens can significantly influence test results. Considering that the specimens used in this paper were 3D-printed, some variations in the results were likely influenced by irregularities in the manufacturing process.
The Digital Image Correlation (DIC) is primarily used to measure linear and shear deformations, and this technique can be applied to any type of material. The advantage of this non-contact technique is that the measurement is three-dimensional [15].
This study aims to evaluate the mechanical behavior of polyethylene terephthalate glycol (PETG) specimens printed at different raster angles, comparing results between contoured and un-contoured specimens. Additionally, the study compares strain measurements obtained using a mechanical extensometer and a Digital Image Correlation (DIC) system. The analysis focuses on tensile and shear performance, highlighting how raster orientation and the presence of a shell contour influence strength, ductility, and failure modes. The results reveal that the contour primarily enhances layer adhesion and structural confinement. The Tsai – Hill failure criterion was used to predict tensile properties for 45° specimen orientations based on the results from tensile strength at 0˚ and 90˚ orientations and shear tests at 45° orientations.

MATERIAL AND METHODS

For the preparation of test specimens, a Prusa 3D printer with a 0.2 mm diameter nozzle was used. The printing temperature was set to 220°C. Specimens were printed in various raster orientations, specifically 0°, [+45°/ -45°], and 90°, to investigate the effects of orientation on mechanical properties. Each specimen was produced in two configurations: with and without a shell contour, enabling an analysis of whether the contour affects the strength and toughness. A 100% infill density was considered to enhance interlayer adhesion and ensure material homogeneity. The other printing parameters were: nozzle diameter 0.2 mm, nozzle temperature 230° C, bed temperature 80° C, and layer thickness 0.02 mm.
Testing was conducted at room temperature using a Zwick ProLine Z005 testing machine equipped with a 5 kN load cell. The cross-head speed was set to 5 mm/min and continued until specimen failure. To ensure accurate strain measurements, a Dantec Digital Image Correlation (DIC) system was used, enabling full-field strain analysis for all specimens.
Six specimens were tested for each orientation, and the average results were reported. The tensile and shear test results were then used for analytical validation using the Tsai-Hill criterion, enabling a comparison between calculated and experimental results.
For each specimen orientation, strain measurements were conducted using both a mechanical extensometer and a digital extensometer. The digital extensometer measurements were performed using a Dantec Q400 system, equipped with two cameras to enable full-field strain analysis. Before testing, all specimens were prepared and coated with white paint. Once dried, black speckles were applied across the specimen's surface to create a high-contrast pattern, ensuring accurate strain tracking by the camera system. All collected data were analyzed to obtain true strain values, ensuring accurate representation of the material's deformation behavior under applied loads.

TENSILE TEST

The specimens were fabricated according to ISO 527-2, as shown in Figure 1. The tensile test was conducted for specimens printed at different raster orientations, with the loading direction relative to filament alignment β. In the 0° orientation, the load was applied along the filament direction; in the 90° orientation, the load was applied perpendicular to the filaments; and in the 45° orientation, the filaments were alternately arranged at +/-45°, Figure 2.
Table 1 presents the filament orientations and contour configurations 0° orientation. In the uncontoured specimens, the edges appear rough and uneven, as no additional material was applied for surface refinement. In contrast, the contoured specimens include two additional outer layers of 0.2 mm, which result in smoother and more uniform edges, enhancing structural cohesion and potentially improving load transfer at the boundaries. For the 45° and 90° orientations, the edge configurations remain consistent, following the same contouring approach as applied to the 0° specimens.

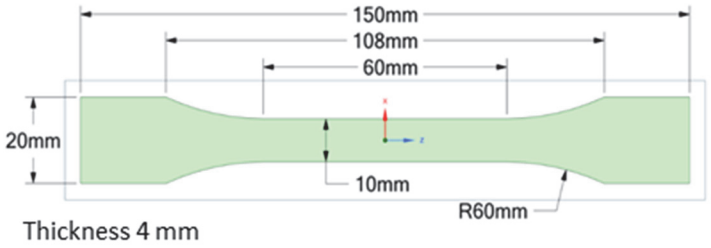

Figure 1: Tensile specimen geometry.

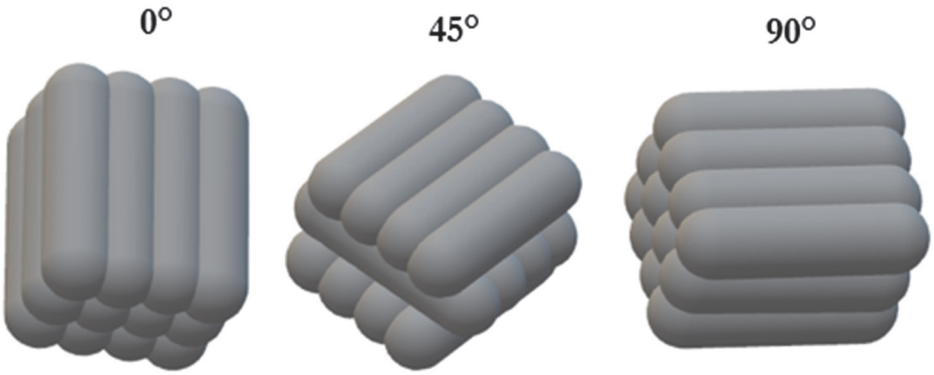

Figure 2: Filament orientation in the specimens.

	Tensile	Shear
Uncontoured	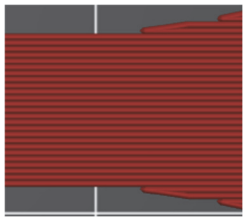	
Contoured	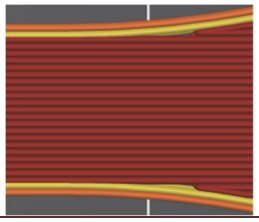	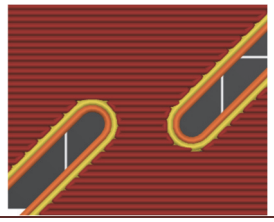

Table 1: Specimens configuration.

After completing the tests and processing the data, the 0^0 orientation exhibited the highest tensile strength compared to the other orientations. The presence of a shell contour did not significantly impact the results for these specimens, as the average tensile strength values were similar. In the uncontoured specimens, the 0° orientation exhibited limited plastic deformation, as evidenced by the corresponding force–displacement curves, Figure 3a. Although they showed higher strength, and exhibited higher toughness comparing with the other orientations.

In contrast, 90° orientation uncontoured specimens produced the weakest fracture energy, Figure 4. As shown in Figure 3b, the 90° orientation exhibited higher tensile strength compared to the 45° orientation. These specimens exhibited brittle failure, with cracks propagating through the layers and breaking the interlayer adhesion. Fracture Energy [Nm] is a critical parameter for describing the fracture behavior of a material. It represents the amount of energy absorbed before the initiation and propagation of a crack. Fracture energy is quantified as the area under the Force-Displacement curve up to the point of failure, providing insight into the material's toughness and resistance to crack growth

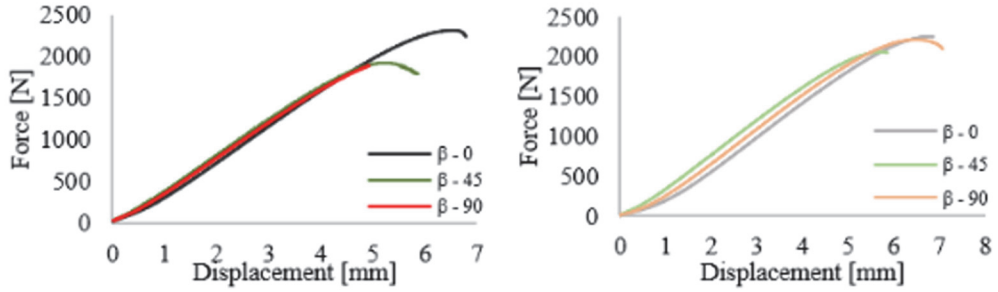

Figure 3: Force – Displacement curves for 0°, 45°, and 90° tensile specimen orientation a) without contour and b) with contour.

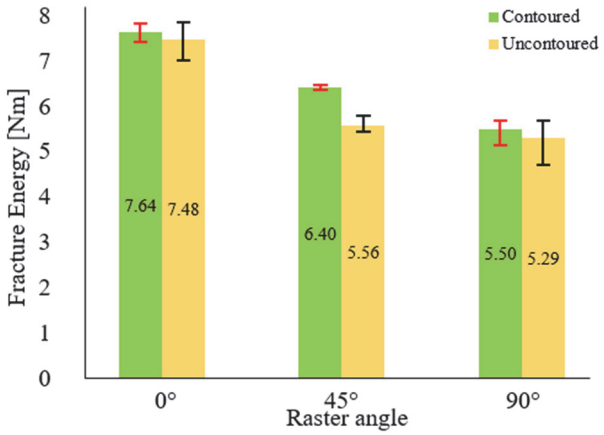

Figure 4: Fracture Energy for all raster orientation.

Figure 5 presents the fractured specimens for all configurations, with the fracture zones magnified for better visualization. In contoured 0° specimens, the material undergoes elongation without visible cracking. In contrast, cracks appear at different angles for other orientations depending on the raster configuration. In the 45° configuration, cracks propagate along a 45° angle, indicating interlayer failure. For 90° specimens, cracks develop horizontally, following the layered structure of the print.

Figure 6 shows the True Stress—True Strain curves extracted from both the extensometer and DIC. There is a good correlation between the curves, as their shapes are very similar. However, the maximum value of the true strain is greater for the contoured specimens 0.05 mm/mm comparing with 0.035 mm/mm for specimens without contour. With the DIC, it was possible to capture a continuous set of data throughout the elongation.

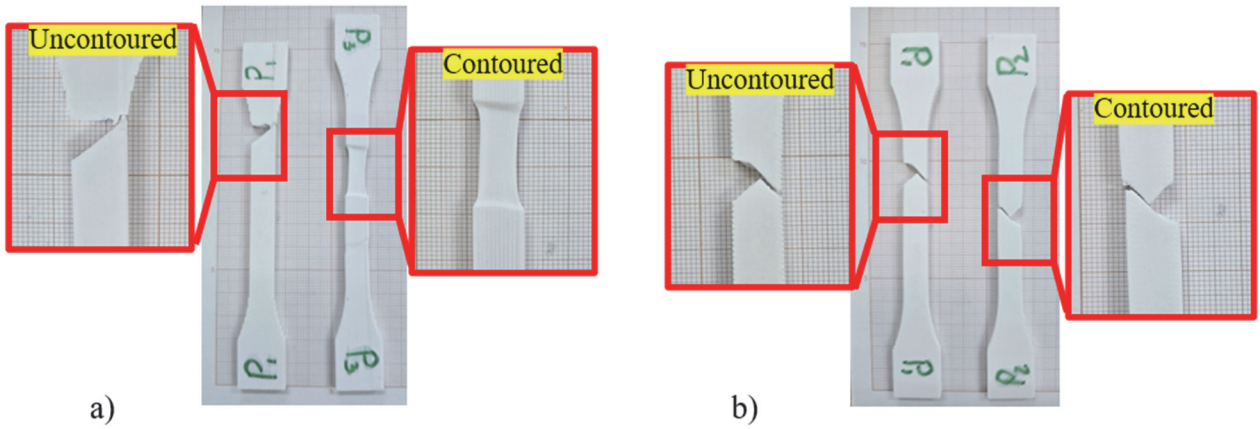

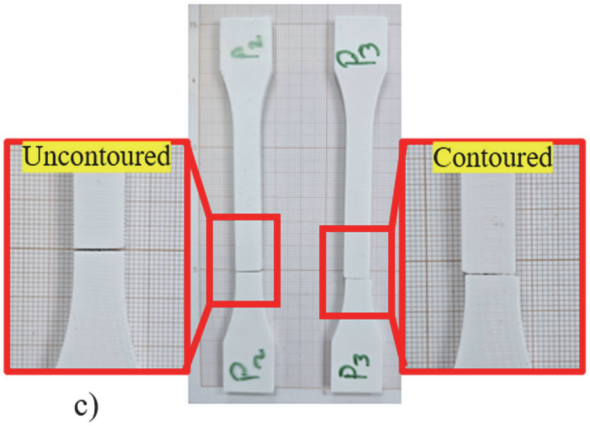

Figure 5: Fracture Tensile Specimens for a) 0°, b) 45°, and c) 90°.

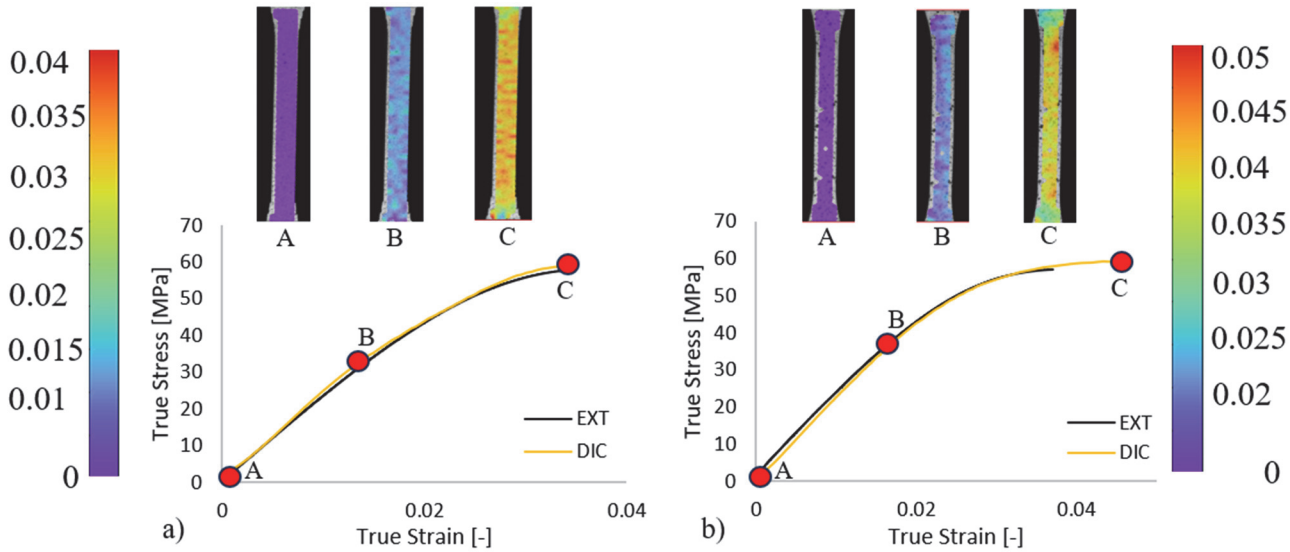

Figure 6: True Stress – True Strain curves for 0° specimen orientation a) without contour and b) with contour.

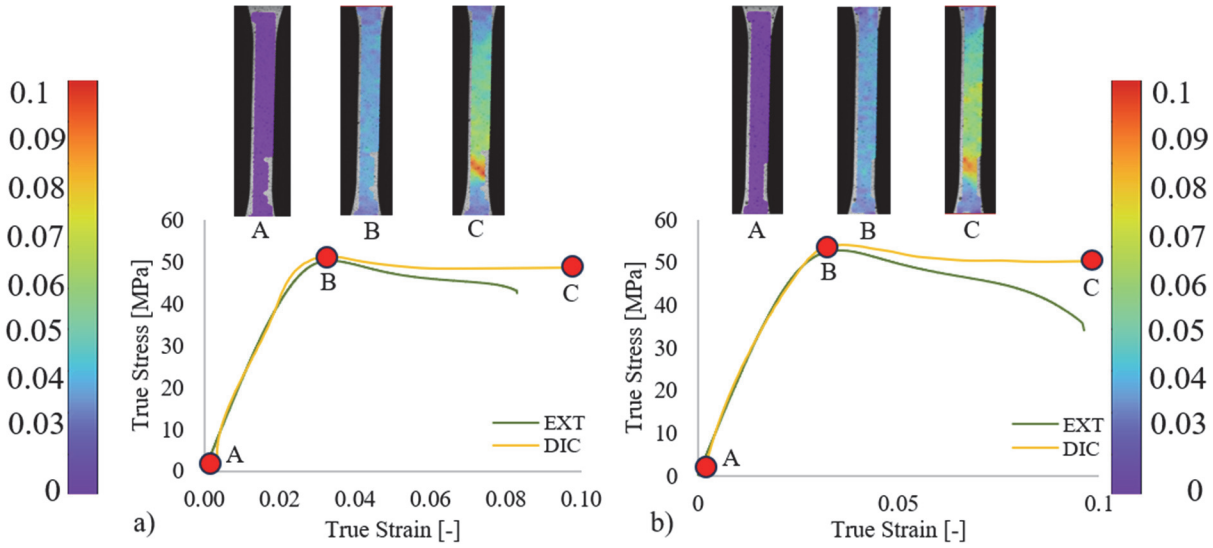

Figure 7: True Stress – True Strain curves for 45° specimen orientation a) without contour and b) with contour.

Figure 7 shows the True Stress – True Strain curves for 45° specimens. In this case, the curves obtained from Digital Image Correlation (DIC) align closely with those from the mechanical extensometer, particularly within the elastic region. However, beyond the elastic limit, where large deformations and localized strain concentrations occur, the extensometer was unable to accurately capture data due to its limited contact-based measurement range and inability to track strain in non-uniform regions. In contrast, the DIC system successfully recorded the strain distribution across the entire gauge length, including the critical elongation zones, thanks to its full-field, non-contact measurement capability.

As mentioned earlier, 90° specimens exhibit brittle behavior, which is also reflected in the true stress–true strain curves, Figure 8. For contoured specimens, some variation in the results was observed. Two specimens showed higher stress values compared to the others. However, one of the curves measured with the extensometer closely aligns with the DIC measurements, demonstrating a good fit.

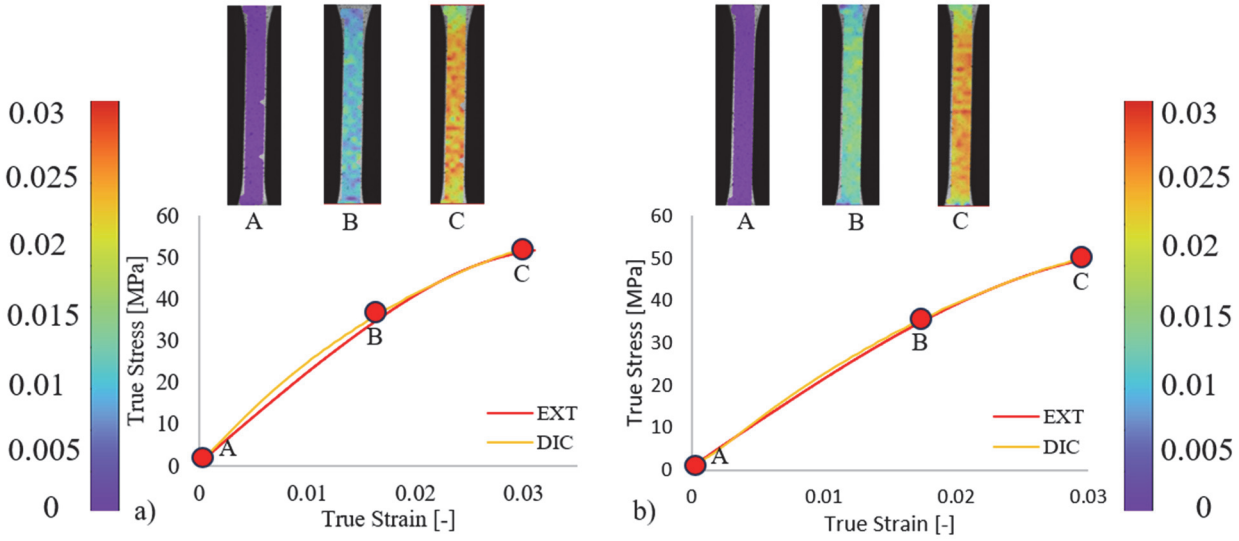

Figure 8: True Stress – True Strain curves for 90° specimen orientation a) without contour and b) with contour.

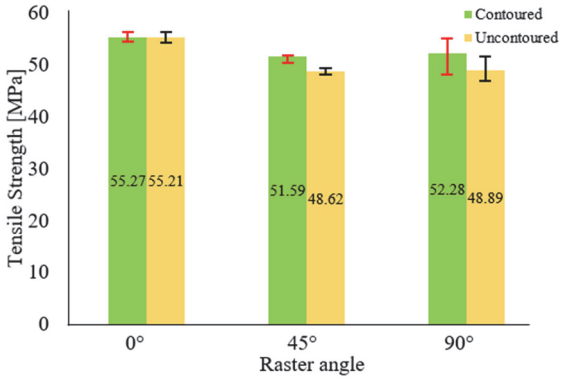

Figure 9: Tensile strength.

The average tensile strength for all specimens is plotted in Figure 9, comparatively for contour and without contour specimens. The plot shows that the tensile strength values for the 0° configuration are nearly independent of the contour of the specimen, due to the fact that the contours are aligned with the printing fibers. Specimens built in a 45° orientation exhibited ductile behavior in tensile. These specimens elongated significantly after reaching the yield point, with cracks initiating only after several millimeters of deformation. They have the minimum tensile strength for both contoured and uncontoured specimens and medium toughness comparing with 0° and 90° orientations. The contour effectively constrained the layers, making crack propagation more difficult and resulting in higher tensile strength, Figure 5.

In contrast, the difference between contoured and un-contoured specimens is more pronounced for 45° orientation in the case of fracture energy. A greater scatter is observed for tensile strength in the 90° orientation results; however, the average of the tensile strength remains higher for the 90° orientation compared to the 45° orientation.

For the contoured specimens, the tensile strength is higher due to the contour orientation along the loading direction.

SHEAR TEST

The shear specimens were fabricated following the ASTM 831-5 standard, which is specifically designed for thin sheet plates, Figure 10.

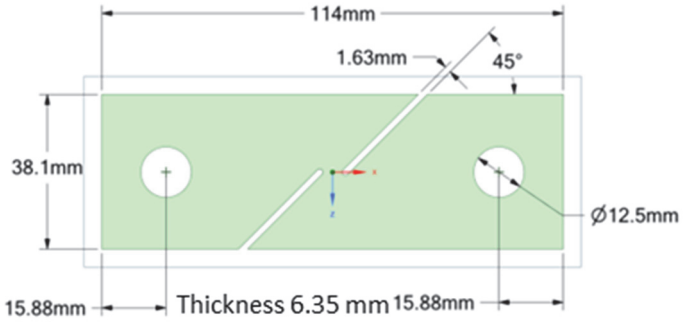

Figure 10: Shear specimen geometry

As in the previous tests, six specimens were tested for each shear configuration. Force-displacement curves were recorded for each configuration (Figure 11), with average values presented for clearer visualization. In the shear test, 0° uncontoured specimens exhibited reduced performance, primarily due to their geometry, specifically, the alignment of filaments with the loading direction, which limited their capacity to resist shear forces compared with the contoured specimens. The 0° contoured specimens showed enhanced mechanical performance, attributed to the reinforcing effect of the shell contour, which helped maintain structural integrity under shear loading. Crack initiation occurred through the layers in the calibration area, Figure 12. The difference in results between contoured and uncontoured specimens was attributed to the contour, which helped maintain layers integrity and allowed the force to increase until the shell eventually broke.

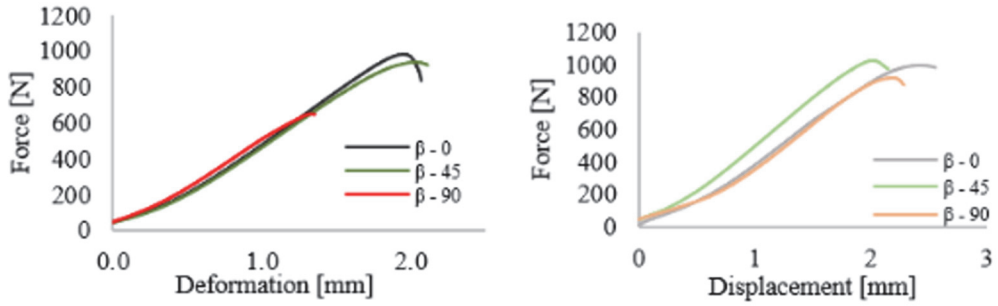

a) b)

Figure 11: Force – Displacement curves for 0°, 45°, and 90° shear specimen orientation a) without contour and b) with contour.

The specimens built in a 90° orientation exhibited a different behavior. Significant deformation was observed in the calibrated area, which continued until reaching a critical force affecting interlayer adhesion. The crack is initiated horizontally along the layers indicating that failure occurred more easily between layers rather than through filament breakage.

The specimens exhibited superior performance in the 45° configuration. Strain was concentrated in the calibrated area, where the crack initiation occurred. The results indicate higher strength and toughness for this configuration.

Crack propagation in shear specimens exhibits different behaviors depending on the raster orientation. Figure 12 presents the fractured specimens for all configurations.

In the 0° configuration, Figure 12a, crack initiation differs between contoured and uncontoured specimens. In uncontoured specimens, the crack initially propagates in the calibrated zone but later deviates along an alternative path. Conversely, in contoured specimens, the crack initiates vertically, breaking the layer adhesion. For the 45° configuration, Figure 12b, cracks develop within the calibrated zone, following the layer orientation. In the 90° configuration, Figure 12c, crack propagation aligns with the printing orientation. In uncontoured specimens, cracks extend in both vertical and horizontal directions. However, in contoured specimens, the contour reinforcement increases specimen strength, causing cracks to propagate horizontally.

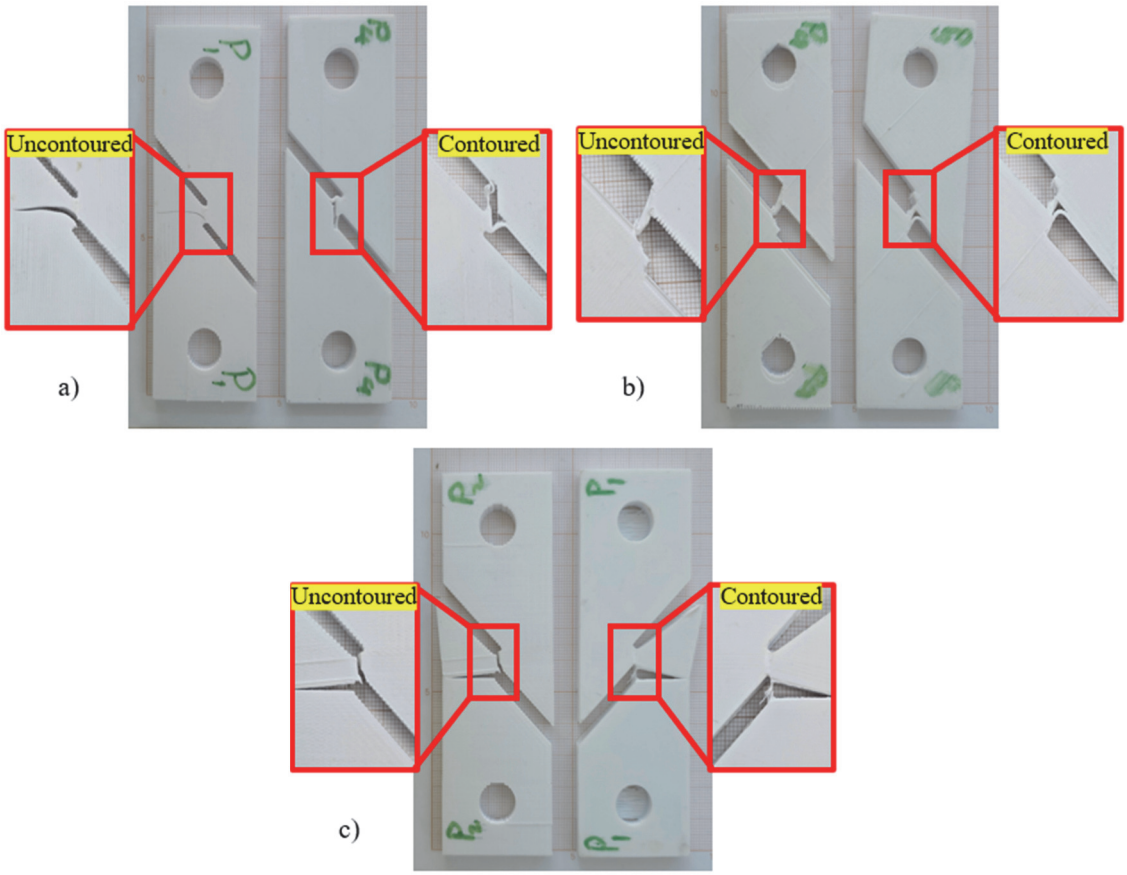

Figure 12: Fracture Shear Specimens for a) 0°, b) 45°, and c) 90°.

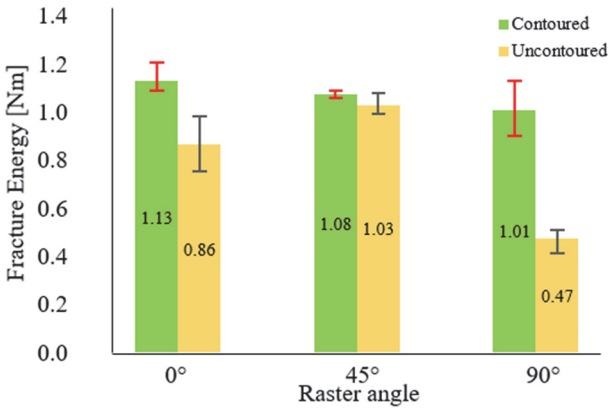

Figure 13: Fracture Energy for all raster orientations.

As previously mentioned, fracture energy was also evaluated for shear specimens, as shown in Figure 13. The values were quantified by calculating the area under the Force-Displacement curve, providing a comparative analysis of the material's energy absorption capacity in different shear configurations.

Figure 14 illustrates the true stress–true strain curves raised from shear tests with strain measurements taken using DIC. However, data extraction was not possible for all specimens due to the poor image quality and the surface inconsistencies. The 90° specimens exhibit significantly lower strain due to their brittle nature. As previously mentioned, these specimens were fractured in areas outside the calibrated zone. Furthermore, un-contoured specimens displayed even lower strain, as their filament orientation facilitated crack propagation. The presence of a contour significantly enhances shear strength. In uncontoured specimens, the true stress–true strain curve exhibits a relatively small plateau region, indicating limited plastic deformation before failure. Conversely, contoured specimens demonstrate greater deformation capacity, attributed to the

contoured specimens. This extended deformation allows for data collection over a longer duration, providing more comprehensive insights into the material's mechanical behavior under shear loading.

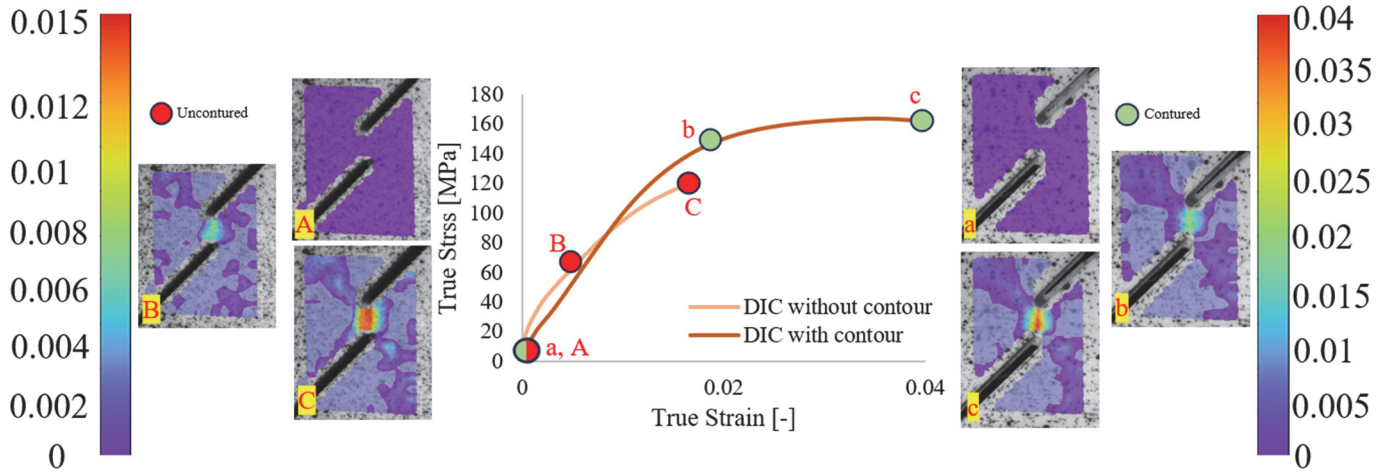

Figure 14: True Stress – True Strain curves for 90^0 orientation.

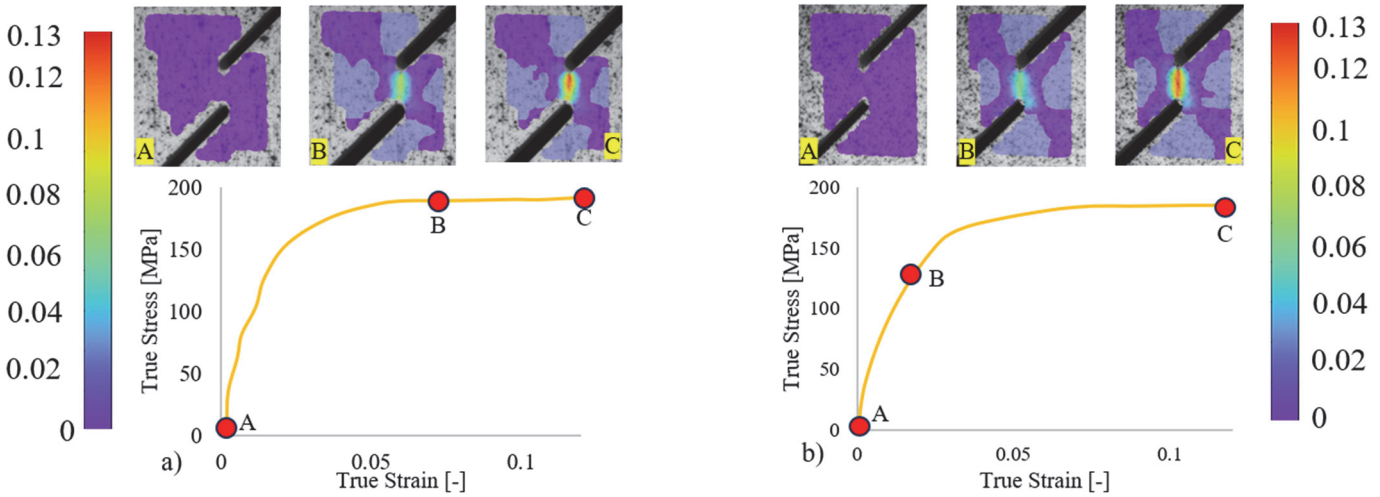

Figure 15: True stress-true strain with pictures from DIC for Shear specimens 0° and 45° orientation.

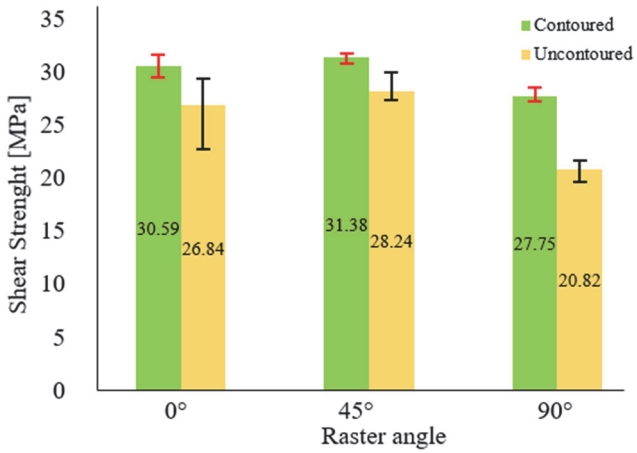

Figure 16: Shear Strength.

Figure 15 presents the true stress–true strain curves for shear specimens accompanied by images depicting strain distribution during testing. In the intermediate frame of the first curve, strain appears localized within the calibrated area. However, for the 45° orientation, strain is initially distributed at ±45° near the calibrated zone. As deformation advances, the strain increasingly concentrated within the calibrated area in the final frame due to the significant deformation.
The shear strength varied depending on the specimen configuration. The highest shear strength was recorded in contoured specimens with a 45° configuration, averaging 31.38 MPa, compared to 28.24 MPa for uncontoured specimens, Figure 16. The lowest shear strength was observed in 90° specimens, where the maximum strength reached only 27.75 MPa with a contour and dropped to 20.83 MPa without contour. For the 0° configuration, contoured specimens exhibited a shear strength of 30.59 MPa, while un-contoured specimens measured 26.83 MPa.

TSAI-HILL CRITERION

The Tsai-Hill failure criterion, developed by Stephen W. Tsai and based on the Hill yield criterion for anisotropic materials, represents a significant advancement in the predictive modeling of composite material failure [16 – 21]. Building upon the foundational Von Mises criterion, designed for isotropic materials, Tsai extended the approach to account for the anisotropic mechanical behavior inherent to composite structures. This refinement bridges the gap between theoretical material strength and practical engineering applications, providing a mathematically efficient and experimentally validated method for assessing the structural integrity of fiber-reinforced composites under complex loading conditions. By enabling engineers to predict failure with high reliability, the Tsai-Hill criterion has become a pivotal tool in advancing the safe and efficient use of composite materials in high-performance applications.
Zhao et al. [20] employed the Tsai-Hill criterion in order to predict the fracture strength of PLA materials printed at different printing angles using FDM technique. They used the tensile strength values at 0°, 45° and 90° to fit the Tsai-Hill criterion. In the present study, tensile tests at 45° are replaced by shear strength at 45^0 raster angle.
The Tsai-Hill equation utilizes the tensile strength values from 0° and 90° specimens, as well as the shear strength from 45° specimens, to predict the tensile strength of 45° specimens, Figure 18. This approach leverages the strengths of materials along different orientations to provide an accurate estimation of the material's behavior under various loading conditions, [20]:

$$\sigma_\theta = \left[\frac{\cos^4\theta}{\sigma_{0^0}^2} + \left(\frac{1}{\tau_{45^0}^2} - \frac{1}{\sigma_{0^\circ}^2} \right) \sin^2\theta \cos^2\theta + \frac{\sin^4\theta}{\sigma_{90^\circ}^2} \right]^{-0.5} \tag{1}$$

σ_{0° - Tensile strength in the longitudinal direction

σ_{90° - Tensile strength in the transversal direction

τ_{45° - Shear strength at 45° orientation.

σ_{θ° - Tensile strength relative to the load direction

The experimentally obtained values are shown in the Table 2. Figure 17 illustrates the specimen orientations and types considered in the application of the Tsai–Hill equation. For the tensile tests, specimens with 0° and 90° orientations were used, while for the shear analysis, only the 45°-oriented specimens were considered, following the requirements of the failure criterion. The average values were used in eq. (1) to calculate the predicted tensile strength at 45°. These predicted values were then compared with the obtained experimental results, Figure 18.
Figure 18 presents the experimental measured tensile strengths and the variation of tensile strength provided by Tsai-Hill criterion. The calculated tensile strength for contoured specimens at 45° orientation using Eq. (1) was 52.95 MPa, whereas the experimentally obtained average value was 51.1 MPa, yielding a 3.5 % relative error. For the unconutured specimens the predicted value with Tsai-Hill criterion is 48.9 MPa, which in very good agreement with the experimental measured value of 48.62 MPa, resulting a 0.6 % relative error. The higher relative error for contoured is because specimens in the shear area have the contour shell with other orientation comparing with the orientation of fibers.

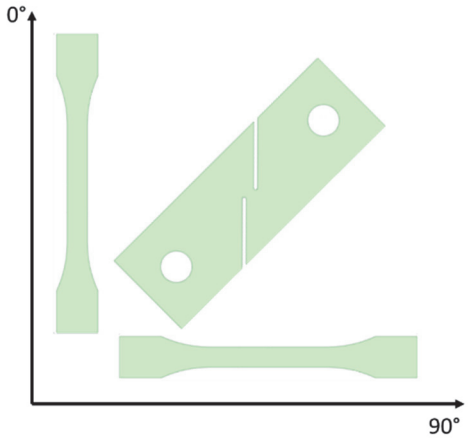

Figure 17: Specimen orientation for Tsai-Hill analysis.

No.	σ_{0^o}		σ_{90^o}		τ_{45^o}	
	Contoured	Un-Contoured	Contoured	Un-Contoured	Contoured	Un-Contoured
1	54.48	54.35	48.92	46.85	31.71	27.32
2	54.56	54.70	48.2	49.09	30.9	28.2
3	54.77	55.18	55.06	47.38	31.36	27.47
4	56.25	56.29	54.92	51.09	31.66	29.95
5	55.70	55	54.29	50.04	-	-
Av	55.26	55.21	52.27	48.89	31.38	28.24

Table 2: Experimental values.

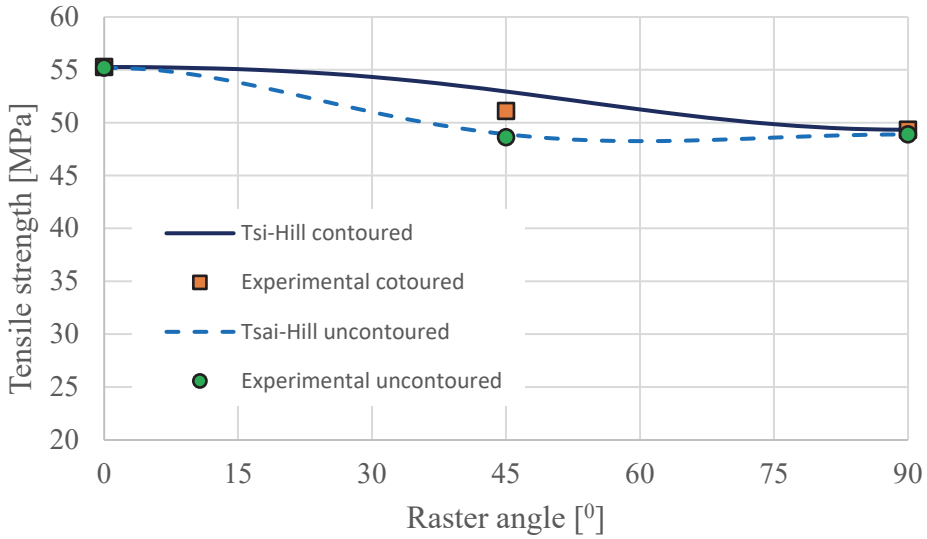

Figure 18: Tensile strength for experimental result and analytical result.

Conclusion

This study investigated the tensile and shear strength of PETG specimens manufactured using FDM at different raster orientations. The results revealed: that 0° orientation specimens exhibited the highest tensile strength and fracture energy. In contrast, 90° orientation specimens had the lowest strength. The specimens with 45° orientation

demonstrated the lower tensile strength. For all orientations contoured specimens highlighted higher strength and toughness, compared with the uncontoured ones.
For the shear tests maximum shear strength was obtained for 45° orientation and the same like in tensile tests the the contoured specimens have higher strength and fracture energy.
Both the extensometer and DIC methods to measure the strains provided accurate results, with only minor discrepancies due to pre-loading effects. The DIC system is particularly advantageous for testing shear specimens and measuring the shear strain, where attaching an extensometer is difficult or impracticable. Despite slight variations at the beginning of the measurement, both methods yielded the same strain values at the point of specimen fracture.
The Tsai-Hill criterion provided an accurate prediction of tensile strength, with only a 3.5% relative error compared to experimental results for contoured specimens, respectively with 0.6 % relative error for uncontoured specimens. This makes the Tsai-Hill criterion a reliable tool to predict the tensile strength of PETG polymers obtained using FDM technique.

ACKNOWLEDGEMENTS

The research leading to these results was partially supported from the European Union's Horizon 2020 research and innovation program (H2020-WIDESPREAD-2018, SIRAMM) under grant agreement No. 857124 and by a grant of the Ministry of Research, Innovation and Digitization, CNCS - UEFISCDI, project number PN-IV-P1-PCE-2023-1446, within PNCDI IV.

REFERENCES

[1] Zhang, P., Arceneaux, D. J., Liu, Z., Nikaeen, P., Khattab, A. and Li, G. (2018). A crack-healable syntactic foam reinforced by 3D-printed healing-agent-based honeycomb. Composites Part B, 151, pp. 25–34.
[2] Malik, H. H., Darwood, A. R., Shaunak, S., Kulatilake, P., Abdulrahman, A., Mulki, O. and Baskaradas, A. (2015). Three-dimensional printing in surgery: A review of current surgical applications. Journal of Surgical Research, 199(2), pp. 512–522.
[3] Mulford, J. S., Babazadeh, S. and Mackay, N. (2016). Three-dimensional printing in orthopaedic surgery: Review of current and future applications. ANZ Journal of Surgery, 86(9), pp. 648–653.
[4] Henriques, B., Pinto, P., Silva, F., Fredel, M., Fabris, D., Souza, J. and Carvalho, O. (2018). On the mechanical properties of monolithic and laminated nano-ceramic resin structures obtained by laser printing. Composites Part B, 141, pp. 76–83.
[5] Ahmed, N. A. and Page, J. (2013). Manufacture of an unmanned aerial vehicle (UAV) for advanced project design using 3D printing technology. Applied Mechanics and Materials, Trans Tech Publications, pp. 970–980.
[6] Kroll, E. and Artzi, D. (2011). Enhancing aerospace engineering students' learning with 3D-printed wind-tunnel models. Rapid Prototyping Journal, 17(5), pp. 393–402.
[7] Marsavina, L., Vălean, C., Marghitaş, M., Linul, E., Razavi, N., Berto, F. and Brighenti, R. (2022). Effect of manufacturing parameters on the tensile and fracture properties of FDM 3D-printed PLA specimens. Engineering Fracture Mechanics, 274, 108766.
[8] Ziemian, C., Sharma, M. and Ziemian, S. (2012). Anisotropic mechanical properties of ABS parts fabricated by fused deposition modeling. In Mechanical Engineering (pp. 159–180). InTech.
[9] Luo-Ke, S., Peng-Cheng, L., Chang-Ru, L., Jia-Xu, Z., Tian-Hao, Z. and Gang, X. (2024). An improved tensile strength and failure mode prediction model of FDM 3D-printed PLA material: Theoretical and experimental investigations. Journal of Building Engineering, 90, 109389.
[10] Josef, K. and Chao, G. (2020). Controlling toughness and strength of FDM 3D-printed PLA components through the raster layup. Composites Part B: Engineering, 180, 107562.
[11] Komori, K. (2023). Predicting ductile fracture during extended Miyauchi shear testing using an analytical model. International Journal of Solids and Structures, 275, 112320.
[12] Bouvier, S., Haddadi, H., Levée, P. and Teodosiu, C. (2006). Simple shear tests: Experimental techniques and characterization of the plastic anisotropy of rolled sheets at large strains. Journal of Materials Processing Technology, 172, pp. 96–103.
[13] Liu, Y., Genevois, P. and Teodosiu, C. (1990). Influence of shear strain as a pre-deformation on the subsequent mechanical properties of A-K steel. Journal of Materials Processing Technology, 21, pp. 51–63.

[14] Matúš, K., František, Š., Martin, H., Martin, S. and Michaela, Š. (2012). The use of an experimental optical technique for investigating shear strains in samples exposed to shear stress beyond the yield point. Procedia Engineering, 48, pp. 264–272.
[15] Rauch, E. F. (1992). The flow law of mild steel under monotonic or complex strain paths. Solid State Phenomena, 23–24, pp. 317–333.
[16] Hill, R. (1947). A theory of the yielding and plastic flow of anisotropic metals. The Hydrodynamics of Non-Newtonian Fluids, 13 November.
[17] Tsai, W. S. (1970). A general theory of strength for anisotropic materials. Air Force Materials Laboratory, Wright-Patterson AFB, Ohio 45433.
[18] Sun, C. T. (n.d.). Strength analysis of unidirectional composites and laminates. Purdue University, West Lafayette, IN, USA.
[19] Talreja, R. (2015). A mechanisms-based framework for describing failure in composite materials. In Structural Integrity and Durability of Advanced Composites.
[20] Zhao, Y., Chen, Y. and Zhou, Y. (2019). Novel mechanical models of tensile strength and elastic properties of FDM AM PLA materials: Experimental and theoretical analyses. Materials & Design, 181, 108089.
[21] Micota D., Isaincu A., Marşavina L. (2021) Experimental testing of two short-fiber reinforced composites: PPA-GF33 and PPS-GF40, Materials Design and Process Communications, 3(6), e264.